J. Fluid Mech. (2000), *vol.* 411, *pp.* 39–58. Printed in the United Kingdom

The effect of boundary properties on controlled Rayleigh–Bénard convection

By LAURENS E. HOWLE

Department of Mechanical Engineering and Materials Science,
and Center for Nonlinear and Complex Systems, Duke University, Durham, NC 27708-0300, USA

(Received 15 February 1999 and in revised form 20 December 1999)

We investigate the effect of the finite horizontal boundary properties on the critical Rayleigh and wave numbers for controlled Rayleigh–Bénard convection in an infinite horizontal domain. Specifically, we examine boundary thickness, thermal diffusivity and thermal conductivity. Our control method is through perturbation of the lower-boundary heat flux. A linear proportional-differential control method uses the local amplitude of a shadowgraph to actively redistribute the lower-boundary heat flux. Realistic boundary conditions for laboratory experiments are selected. Through linear stability analysis we examine, in turn, the important boundary properties and make predictions of the properties necessary for successful control experiments. A surprising finding of this work is that for certain realistic parameter ranges, one may find an isola to time-dependent convection as the primary bifurcation.

1. Introduction

Controlling fluid flow has recently become an area of great interest to the scientific and engineering fields. Generally, flow control can be split into two broad categories – passive or active. Passive flow control involves system changes that require no additional energy input. Gad-el-Hak (1996) divides active control into the two categories of predetermined and reactive. In the controls literature, these two categories are known as feed-forward and feedback. Predetermined active control relies on energy input to the system but requires no knowledge of the flow state. Reactive flow control, on the other hand, adjusts the control input according to the state of the flow. Many of the potential applications of flow control, suppression of turbulence for example, have obvious importance. Other flow control problems, such as the control of Rayleigh–Bénard convection, on which this work focuses, are also motivated by potential practical applications. For example, in Czochralski crystal growth, time-dependent convection in the melt is known to cause inhomogeneities that degrade the properties of finished wafers (Müller 1988). The control of Rayleigh–Bénard convection is a reasonable model problem for flow control in the Czochralski crystal growth process. In this paper, we focus on reactive control of Rayleigh–Bénard convection through perturbation of the heat flux distribution.

Early work on stabilizing or destabilizing the Rayleigh–Bénard system is summarized by Davis (1976) for the cases of periodic gravitational modulation and periodic thermal modulation. For periodic gravitational modulation, the entire convection layer is oscillated vertically so that the gravitational acceleration is the sum of a mean and a harmonic value. Gresho & Sani (1970) used a one-mode Galerkin method to examine this problem and found that positive Rayleigh numbers can be stabilized

while negative Rayleigh number can be destabilized. The case of temporal modulation of the vertical thermal gradient was examined by several investigators, see Venezian (1969), Rosenblat & Herbert (1970), Rosenblat & Tanaka (1971), Yih & Li (1972). Success in delaying convection onset using temporal modulation was found to be marginal.

An active–reactive method for controlling Rayleigh–Bénard convection was proposed by Tang & Bau (1993*a*, *b*, 1994, 1995). Through linear stability analysis and numerical simulations, Tang & Bau showed that a horizontally infinite fluid layer can be stabilized by perturbing the lower thermal boundary condition in proportion to the temperature distribution at the layer's mid-height. Using linear control, Tang & Bau found it possible to delay the onset of convection by up to an order of magnitude. Additionally, they found that a Hopf bifurcation to time-dependent convection may occur if the gain is too great. In an experimental study of convection control in a small-aspect-ratio upright cylinder Tang & Bau (1998) demonstrated the delay of convection onset by shifting the critical Rayleigh number by a factor of approximately 1.5.

In a previous experimental investigation of Rayleigh–Bénard convection control, we used a 0.79 cm high fluid layer of ethylene glycol in a rectangular container with aspect ratio 1×2 (Howle 1997*a*). On the underside of the lower boundary were five individually controlled heaters. We measured the local convection amplitude by a shadowgraph. This shadowgraphic signal was used with a linear proportional control law to actively distribute the lower boundary heating. The control law distributed the heat flux so that the mean flux was constant. The experiments significantly reduced the convection amplitude over the range $1 < R/R_u < 9$ where R is the Rayleigh number and R_u the uncontrolled critical value. However, this experiment was unable to delay the onset of convection (we were unable to move the eigenvalues of the system). In that study, we found that the lower-boundary properties (thickness, thermal conductivity and thermal diffusivity) had a significant influence on the controller success.

In a second experimental investigation (Howle 1997*b*), we refined the apparatus by reducing the feedback delay time and by increasing the fluid layer aspect ratio to 1×6.2. In this experiment, the lower boundary had fifteen individually controlled heaters. With the refined experiment, we controlled convection by shifting the convection onset point to $R/R_u \approx 3.7$. Convection was further suppressed, though weak convection was present, from $3.7 < R/R_u < 8.3$. It is important that we make the distinction between controlling and suppressing convection. In order to control convection, we must move the eigenvalues of the system thus changing its bifurcation point(s). If we suppress convection, we only damp the convection amplitude but do not change the bifurcation point.

Following the experimental work, we used linear stability analysis to study the critical values of a horizontally-infinite fluid layer with proportional control by active perturbation of the lower-boundary Joule heating and with measurement by shadowgraph (Howle 1997*c*). A key finding of the work was that by perturbing the lower heat-flux thermal boundary condition in proportion to the local intensity of the shadowgraphic signal, the convection onset point can be delayed up to $R/R_u = 3.180$. It is the purpose of our present work to extend this linear stability analysis to answer one of the questions posed in Howle (1997*b*): What role do the horizontal boundaries play in determining the critical values for controlled Rayleigh–Bénard convection?

We answer this question through the results of a linear stability analysis of Rayleigh–Bénard convection that includes the horizontal boundaries. The remainder of this paper is arranged as follows: in § 2, we derive the linear stability condition

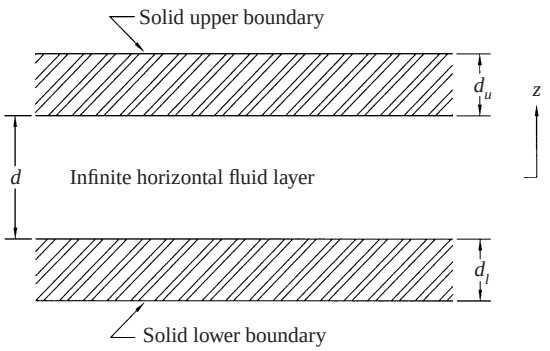

FIGURE 1. The convection layer considered in this problem. The upper and lower bounding planes have thicknesses of d_u and d_l respectively (both scaled by the fluid layer height, d). The ratios of the thermal conductivities of the upper and lower boundaries to the thermal conductivity of the fluid, $\lambda_u = k_f/k_u$ and $\lambda_l = k_f/k_l$ are also important. For Hopf bifurcations to time-dependent convection, the thermal diffusivity ratios $\eta_u = \kappa_u/\kappa_f$ and $\eta_l = \kappa_l/\kappa_f$ play a key role. The feedback control method used in these calculations uses shadowgraphic measurement as the input to an active control system.

for controlled Rayleigh–Bénard convection. The most important part of this stability analysis is the non-local boundary condition through which we impose active control. In § 3, we start by carefully discussing the three types of bifurcations – one stationary and two Hopf – that can occur due to the actuation of our linear controller. This is followed, in § 3.1, by an examination of the influence that the boundary thickness has on the controlled problem with the other parameters fixed. The effect of the thermal conductivity on control is discussed in § 3.2 and this is followed by an examination of the thermal diffusivity effect in § 3.3. In § 3.4, we study differential gain and its influence on the Hopf bifurcations. Finally, we offer concluding remarks and predictions of ideal boundary properties in § 4.

2. Problem formulation

We consider here a Boussinesq fluid bounded by two horizontal planes of finite thickness but infinite horizontal extent as illustrated in figure 1. The bounding planes possess finite, isotropic, constant thermal properties. Specifically, we examine the effect of the boundary thicknesses, $d_{l,u}$ the thermal conductivities, $k_{l,u}$, and thermal diffusivities, $\kappa_{l,u}$ on critical values of Rayleigh–Bénard convection subjected to thermal control with shadowgraphic measurement of the convection amplitude. Here, the subscripts l and u respectively refer to the lower and upper boundaries.

The dimensionless equations of heat conduction in the lower and upper boundaries are

$$\partial_t T_l = \eta_l \Delta T_l \tag{2.1}$$

and

$$\partial_t T_u = \eta_u \Delta T_u. \tag{2.2}$$

The dimensionless parameters $\eta_l = \kappa_l/\kappa_f$ and $\eta_u = \kappa_u/\kappa_f$ in (2.1) and (2.2) are the ratios of thermal diffusivity of the lower and upper boundaries to the thermal diffusivity of the fluid. The Boussinesq equations of mass, momentum and energy conservation in the fluid layer are

$$\nabla \cdot \boldsymbol{u} = 0, \tag{2.3}$$

$$Pr^{-1}\left(\partial_t \boldsymbol{u} + (\boldsymbol{u}\cdot\nabla)\,\boldsymbol{u}\right) = -\nabla p + RT\hat{\boldsymbol{e}}_z + \Delta\boldsymbol{u}, \tag{2.4}$$

$$\partial_t T_f + \boldsymbol{u}\cdot\nabla T_f = \Delta T_f, \tag{2.5}$$

with the Prandtl number $Pr = \nu/\kappa_f$ and the Rayleigh number

$$R = \frac{g\alpha\overline{q}d^4}{\kappa_f \nu k_f} \tag{2.6}$$

where g, α, d, κ_f, ν, and k_f are the respective values of gravitational acceleration, fluid volumetric expansion coefficient, fluid layer height, fluid thermal diffusivity, viscosity, and fluid thermal conductivity. The lower-boundary heat flux, $\overline{q}$, is supplied to the lower side of the lower boundary plate. In scaling (2.1)–(2.5), we use the transport properties of the fluid and take the upper fluid–solid interface temperature as a reference value.

The conduction solution for the system (2.1)–(2.5) is $T = T_l \cup T_f \cup T_u$ with

$$\left.\begin{aligned} T_l &= 1 - \lambda_l(\tfrac{1}{2} + z) && \forall\ z \in [-\tfrac{1}{2} - d_l, -\tfrac{1}{2}],\\ T_f &= \tfrac{1}{2} - z && \forall\ z \in [-\tfrac{1}{2}, \tfrac{1}{2}],\\ T_u &= \lambda_u(\tfrac{1}{2} - z) && \forall\ z \in [\tfrac{1}{2}, \tfrac{1}{2} + d_u], \end{aligned}\right\} \tag{2.7}$$

where we define the thermal conductivity ratios as $\lambda_l = k_f/k_l$, $\lambda_u = k_f/k_u$ and the fluid bath temperature (at the top of the upper boundary) is $T_\infty = -\lambda_u(d_u + Bi^{-1})$. Additionally, $Bi = hd_u/k_u$ is the Biot number and h is the heat transfer coefficient. The linear stability problem is formed by perturbing the solution about the conduction solution (2.7). The perturbation equations for the lower, fluid, and upper regions are respectively

$$\left.\begin{aligned} \sigma\Theta_l &= \eta_l(\mathrm{D}^2 - a^2)\Theta_l,\\ (\mathrm{D}^2 - a^2)(\mathrm{D}^2 - a^2 - \sigma)(\mathrm{D}^2 - a^2 - \sigma/Pr)\Theta_f &= -a^2 R\Theta_f,\\ \sigma\Theta_u &= \eta_u(\mathrm{D}^2 - a^2)\Theta_u. \end{aligned}\right\} \tag{2.8}$$

In (2.8), $\mathrm{D} \equiv \partial_z$, a is the horizontal wavenumber and σ is the growth rate. Equations (2.8) allow the ansatz

$$\left.\begin{aligned} \Theta_l &= A\cosh(x_l z) + B\sinh(x_l z),\\ \Theta_f &= \sum_{i=1}^{3}(C_i\cosh(x_i z) + D_i\sinh(x_i z)),\\ \Theta_u &= E\cosh(x_u z) + F\sinh(x_u z), \end{aligned}\right\} \tag{2.9}$$

where the characteristic values, x_l, x_i, x_u, are the roots of

$$\left.\begin{aligned} x_l^2 &= \sigma/\eta_l + a^2,\\ (x_i^2 - a^2)(x_i^2 - a^2 - \sigma)(x_i^2 - a^2 - \sigma/Pr) + a^2 R &= 0,\\ x_u^2 &= \sigma/\eta_u + a^2. \end{aligned}\right\} \tag{2.10}$$

Boundary conditions for these calculations are meant to match boundary conditions typically found in experiments. Therefore, we take no penetration

$$(\mathrm{D}^2 - a^2 - \sigma)\Theta(\pm\tfrac{1}{2}) = 0 \tag{2.11}$$

and no slip

$$\mathrm{D}(\mathrm{D}^2 - a^2 - \sigma)\Theta(\pm\tfrac{1}{2}) = 0 \tag{2.12}$$

conditions for the fluid velocity. Continuity of temperature

$$\left.\begin{aligned}\Theta_l(-\tfrac{1}{2}) - \Theta_f(-\tfrac{1}{2}) = 0,\\ \Theta_u(\tfrac{1}{2}) - \Theta_f(\tfrac{1}{2}) = 0,\end{aligned}\right\} \tag{2.13}$$

and heat flux

$$\left.\begin{aligned}\mathrm{D}\Theta_l(-\tfrac{1}{2}) - \lambda_l \mathrm{D}\Theta_f(-\tfrac{1}{2}) = 0,\\ \mathrm{D}\Theta_u(\tfrac{1}{2}) - \lambda_u \mathrm{D}\Theta_f(\tfrac{1}{2}) = 0,\end{aligned}\right\} \tag{2.14}$$

at the lower and upper fluid–solid interfaces provide four of the six thermal boundary conditions needed. On the upper side of the top boundary we impose a convective thermal boundary condition

$$\mathrm{D}\Theta_u(\tfrac{1}{2} + d_u) + Bi\,\Theta_u(\tfrac{1}{2} + d_u) = 0. \tag{2.15}$$

Note that $Bi \gg 1$ implies a boundary condition approaching that of constant temperature. This condition is met in most convection experiments but we choose to retain the Biot number here for generality.

The sixth thermal boundary condition is the foundation of the present control method. We set the spatial distribution of the heat flux at the bottom of the lower plate proportional to the local shadowgraphic signal and proportional to the time derivative of the local shadowgraphic signal. This aids the natural dissipation of the problem by increasing the heating to the cool fluid regions and decreasing the heating to the warm fluid regions. In dimensional form, we may write this conditions as

$$q = \bar{q}\left(1 + \left(g_p + g_d\partial_t\right)\frac{\delta\rho}{\rho_0}\right). \tag{2.16}$$

In (2.16), q, $\bar{q}$, g_p, g_d, and ρ are respectively the heat flux supplied to the bottom of the lower boundary, spatially-averaged heat flux, dimensionless proportional gain, differential gain (with units of time) and shadowgraphic signal. To express the shadowgraph signal as a function of the temperature in the fluid, we use the equation derived by Thess & Orszag (1995)

$$\frac{\delta\rho}{\rho_0} = -2H\left(\frac{\mathrm{d}n_0}{\mathrm{d}T}\right)(\partial_x^2 + \partial_y^2)\int_{z=0}^{z=d} T(x, y, z)\,\mathrm{d}z \tag{2.17}$$

where n_0 is the fluid index of refraction at the reference state and H is the distance from the convection layer to the image plane (assumed to be much greater than d). Equation (2.17), which is insensitive to odd modes, assumes that the temperature-dependent index of refraction has the simple form

$$n(T) = n_0 + \frac{\partial n}{\partial T}(T - T_0) \tag{2.18}$$

with $\partial n/\partial T$ constant. This assumption is similar to the Boussinesq approximation used in equation (2.4). In writing (2.17) we have multiplied the right-hand side by -1 to make this expression consistent with experiments. The dimensionless form of (2.16) in terms of the perturbation temperature amplitude and by use of (2.17) is

$$\mathrm{D}\Theta_l(-\tfrac{1}{2} - d_l) = -\lambda_l a^2(\gamma + \xi\sigma)\int_{-1/2}^{1/2}\Theta_f\,\mathrm{d}z \tag{2.19}$$

where

$$\gamma = 2g_p \frac{H}{d} \partial_{\Theta_f} n_0 \tag{2.20}$$

is the scaled proportional gain and

$$\xi = 2g_d \frac{\kappa_f H}{d^3} \partial_{\Theta_f} n_0 \tag{2.21}$$

is the scaled differential gain. See Howle (1997*c*) for a discussion of the limiting assumptions of this equation in the context of feedback control.

Upon substituting the ansatz (2.9) into the boundary conditions (2.11)–(2.15) and (2.19) we obtain the solvability condition for this linear stability problem

$$\mathscr{D} = 0 \tag{2.22}$$

where $\mathscr{D}$ is the determinant of the resulting 10×10 linear system. When $\mathrm{Re}(\sigma) = 0$, (2.22) represents the condition for the neutral state. We solve this problem using a continuation method. This method locates the branch and turning points of the bifurcation diagram (solution curves). We then continue the solutions from the branch or turning points to complete the solution diagram. By parameterizing the solution curve with arc-length along the solution curve rather than treating one of the variables as an independent variable, the continuation method can trace the solution curve past points at which the implicit function theorem is violated – turning points, for example. The reader is referred to Kubiček & Marek (1984) for further details on continuation methods.

3. Results and discussion

The parameter space of this problem is quite large, too large in fact to fully explore here. In an attempt to reduce the size of the parameter space we will only consider cases in which the boundary properties are symmetric. This means that we set $d_l = d_u$, $\eta_l = \eta_u$, and $\lambda_l = \lambda_u$. Further, in most convection experiments, there is good 'thermal contact' between the upper boundary and the cooling bath (see, for example, Howle 1997*b*). This is equivalent to taking $Bi \gg 1$ in (2.15). For this reason, we will use the value $Bi = 10$ for the remainder of this paper. Finally, since we intend to focus on the role of the boundary materials properties, the Prandtl number of the fluid will be set to $Pr = 6.0$ throughout this paper. This Prandtl number is equivalent to that of water at room temperature. These restrictions leave us to explore proportional gain, γ, differential gain, ξ, boundary thickness ratio, $d_{l,u}$, thermal conductivity ratio, $\lambda_{l,u}$, and thermal diffusivity ratio, $\eta_{l,u}$.

Depending on the gain and the other parameters, this system can lose stability either through a real eigenvalue to stationary convection or through an imaginary eigenvalue ($\mathrm{Im}(\sigma) \neq 0$) to time-dependent convection. Further, the time-dependent (Hopf) state can occur through one of two possible mechanisms. In figure 2, we show two neutral curves for a gain of $\boldsymbol{G} = \{\gamma, \xi\} = \{35.676, 0\}$ the minima of which correspond to critical points. We choose this gain so that both minima share the critical Rayleigh number, $R_c = 3389.5$, where the subscript c refers to the critical state. The other parameters, which we treat as independent variables, are $d_u = d_l = 0.44$, $\lambda_u = \lambda_l = \eta_u = \eta_l = 1.0$. We choose this boundary thickness because, as we will show, it displays an interesting bifurcation sequence. The uncontrolled ($\gamma = 0$) critical state for this same set of boundary parameters is $Ra_c = 1257.2$ with a wavenumber $a_c = 2.3635$. The solid curve in figure 2 shows loss of stability through a simple eigenvalue to stationary convection.

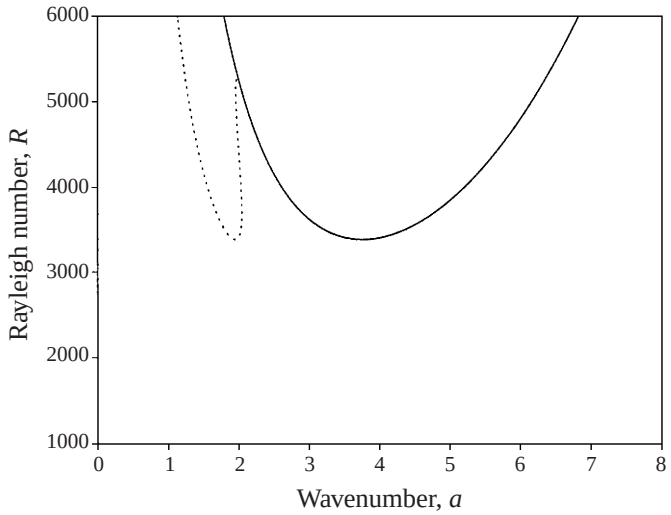

FIGURE 2. Neutral curves for the controlled Rayleigh–Bénard problem with horizontal boundaries. The solid curve corresponds to loss of stability through a real eigenvalue to stationary convection while the dashed curve corresponds to loss of stability through a complex eigenvalue ($\sigma = 19.318\mathrm{i}$) to time-dependent convection. The minima of these curves are the critical points. Conductivity and diffusivity ratios for these solutions are $\lambda_{l,u} = \eta_{l,u} = 1.0$, and the lower and upper boundary thicknesses are $d_{l,u} = 0.44$. For these solutions, we use proportional gain $\gamma = 35.676$ and differential gain $\xi = 0$.

Conversely, the dashed curve shows loss of stability through a complex eigenvalue to time-dependent convection. The solution branches are connected at a codimension-2 point the coordinates of which are $a_2, R_2, \sigma_2 = 1.9764, 5320.6, 0$. Here, the subscript 2 refers to the codimension-2 point. The respective wavenumbers for the Hopf and real critical points are $a_c = 1.9461, 3.7589$. If one decreases the proportional gain, the Hopf branch moves upward while the real branch moves downward. Consequently, loss of stability is through a real eigenvalue and the convection system bifurcates from the conduction state to stationary convection. Conversely, if one increases the proportional gain, the Hopf branch moves below the real branch and loss of stability is through an imaginary eigenvalue to time-dependent convection. When the primary bifurcation is Hopf and the Hopf curve is connected to the real curve by a codimension-2 point, we will call this loss of stability through an H_2 bifurcation. Likewise, we will label a bifurcation to stationary convection as a type S bifurcation. At this gain, where the real and Hopf branches have the same critical Rayleigh number, the system may exhibit complicated behaviour as pointed out by Tang & Bau (1994).

The second type of Hopf bifurcation occurs through the appearance of an isola. This situation is shown in figure 3. The parameters of this solution are identical to the parameters of the H_2 state in the preceding paragraph except that we increase the gain to $\boldsymbol{G} = \{38.092, 0\}$. Figure 3 shows the neutral curve for loss of stability through a real eigenvalue as the solid line. The broken line shows loss of stability through a Hopf bifurcation to time-dependent convection (H_2 curve). The isola, shown as a solid point, corresponds to an isolated complex-eigenvalued solution. We will refer to this type of time-dependent critical point as an H_i bifurcation. For these parameter values, the isola does not exist for a proportional gain below 38.092. A rather remarkable feature of the isola birth point is the existence of this *single* point of linear instability.

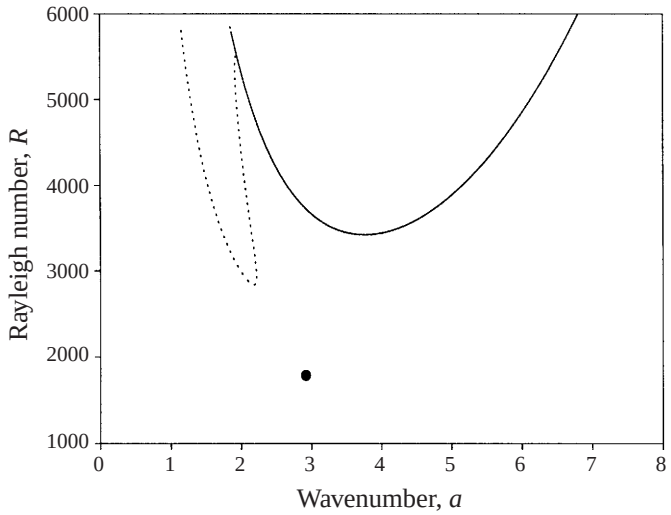

FIGURE 3. Neutral curves for the controlled Rayleigh–Bénard problem including the effect of the horizontal boundaries. The three solutions shown in this figure correspond to loss of stability through a simple bifurcation (solid curve), through a complex bifurcation to time dependent motion (dashed curve) and through an isola to time-dependent motion (solid point). The parameters used for these solutions are $d_{l,u} = 0.44$, $\lambda_{l,u} = \eta_{l,u} = 1.0$, $Pr = 6.0$, and $Bi = 10$. The proportional gain, which we find to locate the isola, is 38.092. For these parameters, the isola is the critical state which has the values $a_c, R_c, \sigma_c = 2.9210, 1787.0, 33.784\text{i}$. Differential gain is not used for these solutions.

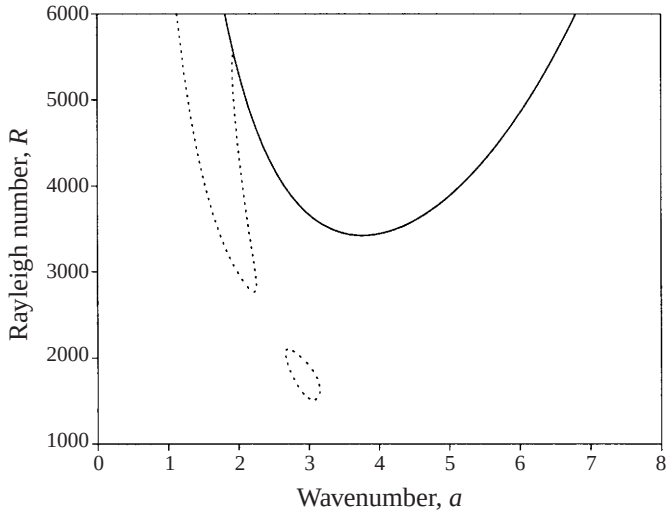

FIGURE 4. Opening of the isola for proportional gain $\boldsymbol{G} = \{38.2, 0\}$, slightly above the gain required to produce the isola in figure 3. The remaining parameters are identical to those used in figure 3. The critical values for this set of parameters are $a_c, R_c, \sigma_c = 3.0608, 1511.0, 36.009\text{i}$.

For gains close to but greater than the gain for isola formation, a small island of R, a space is unstable. This fact should make experimental investigation of the isola birth point possible.

As the proportional gain increases above 38.092, the isola opens into the closed curve shown in figure 4. Since this closed curve occurs through the opening of an

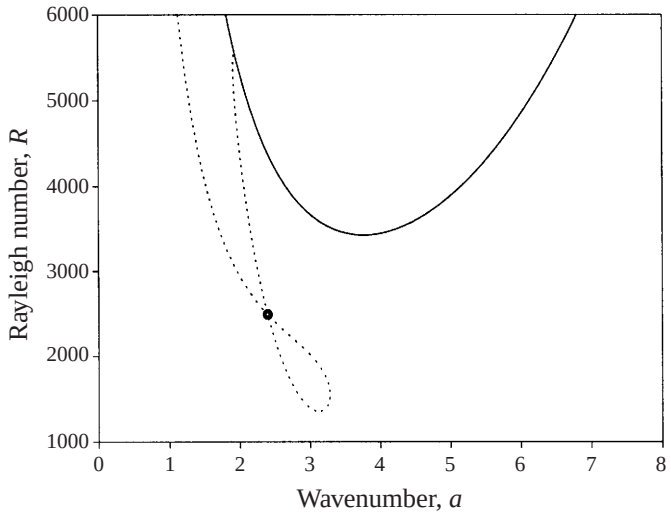

FIGURE 5. Neutral curves showing the location of a saddle point on the Hopf branch (point) with coordinates $a, R, \sigma = 2.3967,\ 2489.1,\ 26.810\mathrm{i}$. The critical values are $a_c, R_c, \sigma_c = 3.1220,\ 1354.4,\ 37.123\mathrm{i}$. The gain for this state is $\boldsymbol{G} = \{38.359, 0\}$.

isola, we will refer to this type of critical state, also, as an H_i bifurcation. As the isola opens, the stationary solution branch shifts slightly upward and the remaining complex solution moves slightly downward. Upon further increasing the proportional gain, the isolated solution branch joins the H_2 branch at a saddle point as shown in figure 5. At this point, the critical state changes from H_i to H_2. For gains greater than that required to produce the saddle point, the H_2 solution branch is continuous and smooth. The possibility of isola formation calls for some care in interpreting the critical points in convection control problems as the isola can occur before the H_2 critical state and can be far-removed from the other neutral stability curves.

To find the isola, figure 3, or the saddle point, figure 5, we must satisfy the system

$$\mathscr{D} = \partial_R \gamma = \partial_a \gamma = 0. \tag{3.1}$$

We solve this system by Newton iteration on the linear system

$$\begin{bmatrix} \partial_R^2 \gamma & \partial_{Ra} \partial_a \gamma \\ \partial_{Ra} \partial_a \gamma & \partial_a^2 \gamma \end{bmatrix} \begin{Bmatrix} \Delta R^n \\ \Delta a^n \end{Bmatrix} = \begin{Bmatrix} -\partial_R \gamma \\ -\partial_a \gamma \end{Bmatrix} \tag{3.2}$$

with

$$\begin{Bmatrix} R^{n+1} \\ a^{n+1} \end{Bmatrix} = \begin{Bmatrix} R^n \\ a^n \end{Bmatrix} + \begin{Bmatrix} \Delta R^n \\ \Delta a^n \end{Bmatrix} \tag{3.3}$$

where all derivatives in the Jacobian matrix and the right-hand-side vector must be evaluated on the solution surface (implicitly) in order to satisfy the marginal stability condition $\mathscr{D} = 0$. The sign of the determinant of the Jacobian matrix distinguishes between a saddle point

$$\partial_R^2 \gamma \partial_a^2 \gamma - (\partial_R \partial_a \gamma)^2 < 0 \tag{3.4}$$

and an isola

$$\partial_R^2 \gamma \partial_a^2 \gamma - (\partial_R \partial_a \gamma)^2 > 0. \tag{3.5}$$

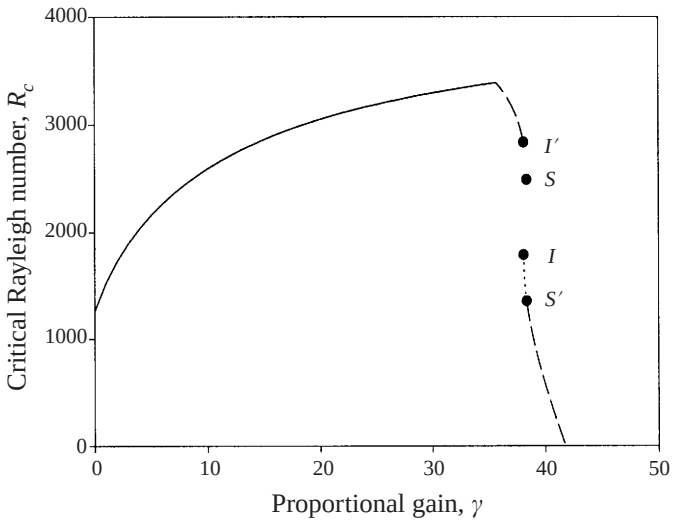

FIGURE 6. Dependence of the critical Rayleigh number on proportional gain. The boundary thickness for these solutions is $d_{l,u} = 0.44$, as with the previous solutions. The thermal transport properties are $\lambda_{l,u} = \eta_{l,u} = 1.0$. At a gain of $\boldsymbol{G} = \{35.676, 0\}$ the maximum critical Rayleigh number is $R = 3389.5$ compared with an uncontrolled critical value of $R_u = 1257.2$. At this point, where the simple (solid curve) and Hopf (dashed curve) branches intersect, the respective critical wavenumbers are $a_c = 3.7589$ and $a_c = 1.9461$. The saddle and isola points are labelled S and I. The portion of the Hopf curve between the points I and I', which includes the point S, is not realizable by this system. Between I and S' (dotted curve) the primary bifurcation is through an isola birth point to time-dependent convection.

The reader is referred to Kubiček & Marek (1984) for a detailed discussion of isola and saddle points.

In figure 6, we show the critical Rayleigh number plotted against the proportional gain, γ. To produce this curve, or any other critical curve, we must track all possible critical points. The critical state, then, is determined by the critical point with the minimum Rayleigh number. The three curves in figure 6 show a type S bifurcation (solid curve), an H_2 bifurcation (dashed curve) and an H_i bifurcation (dotted curve). As the gain increases past $\gamma = 35.676$, the bifurcation changes from S to H_2. As the gain exceeds $\gamma = 38.092$, the critical Rayleigh number takes a discontinuous decrease from $R_c = 2837.5$ to $R_c = 1787.0$. This corresponds to the birth of the isola shown in figure 3. In the region $38.092 < \gamma < 38.359$, the H_i bifurcation persists. At $\boldsymbol{G} = \{38.359, 0\}$, the gain value required to produce the saddle point, the two Hopf branches join and the bifurcation mechanism changes from H_i back to H_2 with increasing gain. This H_2 state survives for $\gamma > 38.359$. Further, for proportional gains greater than 41.779, the critical Rayleigh number is negative. In this case, even with a stabilizing thermal gradient (heating from above), the system can be driven into convection due to the influence of the controller.

The points labelled I and S in figure 6 show the locations of the isola and saddle points respectively. For reference, we also show points I' and S'. These primed points have the same gain as (are conjugate to) their unprimed counterparts. The point I' is the minimum of the H_2 curve at the gain for which the isola appears. Note that the points S and S' lie to the right of I and I'. The portion of the Hopf solution curve (not shown) between I and I' – which passes through S – is not realizable by this system. This is so because the solution below I is unstable for

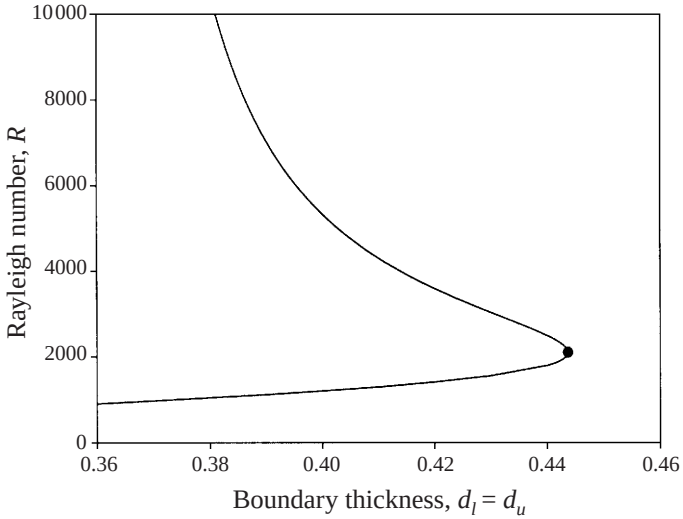

FIGURE 7. Dependence of the Rayleigh number location of the saddle (upper curve) and isola (lower curve) on boundary thickness. For these solutions the thicknesses of the upper and lower boundaries are equal. The point at which the two curves join, shown by the solid point, has the location $a, R, \sigma = 2.6606, 2091.8, 29.853\mathrm{i}$, The gain vector for this point is $\boldsymbol{G} = \{37.682, 0\}$ and the boundary thickness is $d_{l,u} = 0.4437$.

lower Rayleigh numbers. The fact that this portion of the curve is not realizable would be overlooked if one fails to track the location of all three (S, H_2, H_i) critical points. At the point S', the point conjugate to S, the bifurcation changes from H_i to H_2 with increasing gain. We should also stress that one or more of these critical points may not exist for all values of boundary property, gain, or for all Prandtl numbers.

The locations of the isola birth and saddle points depend on the transport property ratios, $d_{l,u}$, $\lambda_{l,u}$, and $\eta_{l,u}$. The points also depend on the Prandtl number; however, we only investigate the case $Pr = 6.0$ at present. We show the dependence of the isola birth point (lower curve) and saddle point (upper curve) on the boundary thickness ratio $d_{l,u}$ in figure 7. For the solutions of this figure, we fix the conductivity and diffusivity ratios at unit values. At the point where the saddle and isola curves intersect, the solution branches annihilate one another at a higher-order singularity. This higher-order isola birth point (HOIBP) is shown as the solid point in figure 7. The most significant fact to be gleaned from figure 7 is that for boundary thickness ratios greater than the thickness ratio corresponding to the HOIBP, there can be no H_i bifurcation. However, there can be an H_2 bifurcation for sufficient gain values. This is an important point for experiment or apparatus design.

The mathematics of locating the HOIBP is non-trivial. Although the linear system (3.2) must be satisfied on the saddle and isola branches (also at the HOIBP), the system is singular at the HOIBP. We find that mathematical methods for dealing with singular systems – for example, singular value decomposition – not to be particularly helpful. The fact that the linear system (3.2) violates the implicit function theorem is useful however. In other words, the determinant of (3.2) vanishes at the HOIBP (see (3.4) and (3.5)). Therefore, a method for creating an augmented system with full rank is by use of the eigenvectors of (3.2). At the HOIBP, one of the two eigenvectors

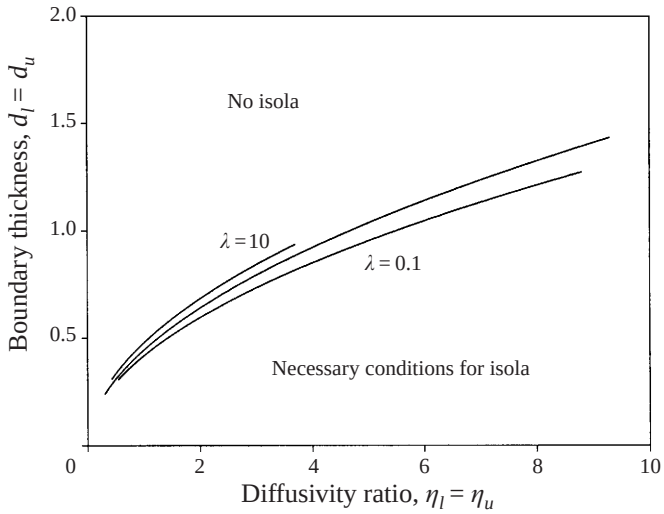

FIGURE 8. Location of a higher-order isola birth point as a function of diffusivity ratio, $\eta_{l,u}$, and boundary thickness ratio, $d_{l,u}$, for three different conductivity ratios, $\lambda_{l,u} = 10^{-1}, 10^{0}, 10^{1}$. For property combinations above the corresponding curve, there is a guarantee of no system bifurcation through isola birth to Hopf convection.

undergoes inflection. Therefore, we use the condition

$$\frac{\partial^2 \gamma}{\partial e_1^2} = 0 \tag{3.6}$$

where the curvature (3.6) must be evaluated implicitly (on the solution surface). In (3.6), e_1 is the direction associated with the inflecting eigenvector. This solution method for locating the HOIBP is robust and relatively straightforward.

Using the methods for locating the HOIBP discussed in the preceding paragraph, we can track the point as we use two of the three transport property ratios as independent variables and treat the remaining transport property ratio as a dependent variable. By choosing the diffusivity and conductivity ratios as independent variables, we find the thickness ratio for which the HOIBP occurs. We show curves of HOIBP location for three values of conductivity ratio, $\lambda = 10^{-1}, 10^{0}, 10^{-1}$ in figure 8. Note that the dependence of the HOIBP on conductivity ratio is relatively weak. For points above the curves, we have the guarantee that the primary bifurcation of the controlled Rayleigh–Bénard system will have either a stationary or a Hopf bifurcation through codimension-2. Hopf bifurcation through an isola birth point, H_i, cannot exist for points above these curves. With the three possible critical points defined and characterized, we are now in a position to explore the effect of the boundary properties on the critical state of the controlled problem.

3.1. *Boundary thickness*

The first parametric study we consider is the set of neutral curves for the critical Rayleigh number as a function of both the proportional gain and the boundary thickness. For these results, the transport properties of the boundary material are set equal to the fluid, $\eta = \lambda = 1.0$. Next, we fix the boundary thickness and use the proportional gain as the independent variable in our continuation method to produce curves of the critical Rayleigh number similar to figure 6. This process is repeated for

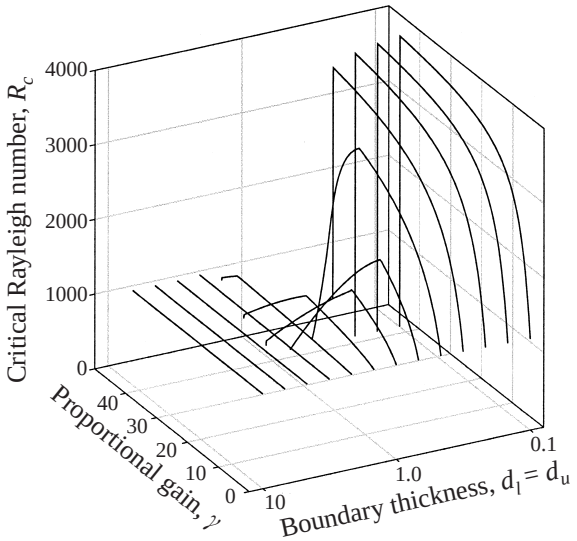

FIGURE 9. Critical Rayleigh number plotted against proportional gain and boundary thickness. For these data, the upper and lower boundaries have the same thickness. The conductivity and diffusivity ratios are constant and equal to 1.0. This figure shows that increasing the thickness of the boundaries generally lowers the maximum critical Rayleigh number. At $\gamma = 0$, the critical values depend on boundary properties and may, therefore, not reproduce the classical Rayleigh–Bénard results. The critical Rayleigh number may be negative for large gain. In this case even a stabilizing thermal gradient, if not sufficiently large, can lead to convection.

twelve uniform increments in $\log(d)$ space over two decades. We show these results in the waterfall plot of figure 9. All three types of critical points are present in the figure. Curves for which R is continuous but the slope of R contains a point of discontinuity have the transition $S \rightarrow H_2$ on increasing γ. Curves for which both R and $\partial_\gamma R$ are discontinuous (shown as a vertical line the figure) display the transition $S \rightarrow H_i$ as γ increases. The transition shown in figure 6, $S \rightarrow H_2 \rightarrow H_i \rightarrow H_2$, exists in a relatively narrow range of boundary thickness and is not shown in figure 9.

The mechanism of loss of stability through Hopf bifurcations depends not only on the gain but also on the boundary thickness. We may interpret this physically if we consider lower-boundary vertical thermal diffusion time. If we increase the thermal diffusion time by increasing the lower-boundary thickness or by reducing the lower-boundary thermal diffusivity then we increase the actuator delay. That is, we increase the amount of time it takes for a change in the heat flux profile imposed on the lower-boundary to reach the fluid. As is well known from control theory, actuator delay can lead to oscillatory (overstable) instabilities. Later we will show that changing η or adding differential gain can also affect the location of the Hopf bifurcations.

The boundary thickness of most precision convection experiments is near to or greater than the upper limit of boundary thicknesses considered here. For example, Howle, Behringer & Georgiadis (1997) used a $d_l = 4.2$ thick copper block for a lower boundary and a $d_u = 0.7$ thick sapphire window for an upper boundary. For this experiment, the large thermal conductance, heat capacity, and thickness of the lower boundary, when compared to the fluid, produced a thermal boundary condition at the lower fluid–solid interface ($z = -\frac{1}{2}$) that was approximately constant temperature rather than the constant flux supplied to the bottom of the lower boundary. The

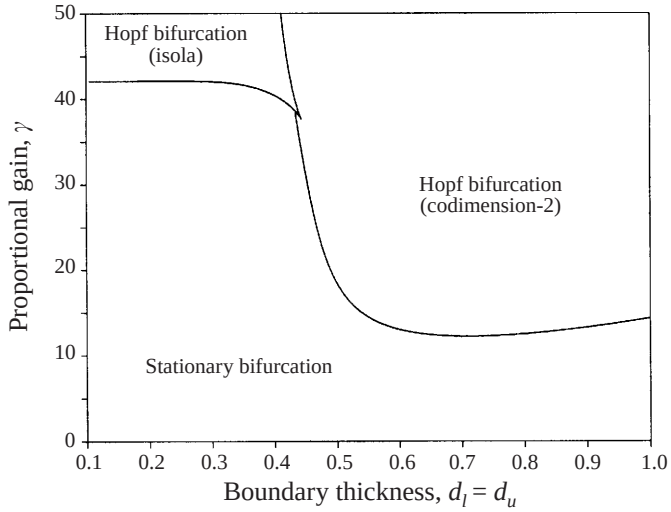

FIGURE 10. Phase diagram for the primary bifurcation type using the proportional gain and boundary thickness as independent variables. For this set of solutions, the conductivity and diffusivity ratios are fixed at 1.0.

influence of the boundary properties on the critical numbers was examined by Metcalf & Behringer (1990) and later by Cerisier *et al.* (1998) for Rayleigh–Bénard convection and by Gustafson & Howle (1999) for convection in porous media. For control of convection through perturbation of the lower heat flux, however, a thick lower boundary has an adverse affect on the maximum critical Rayleigh number. This point is evident upon examining figure 9. The figure shows that as the boundary thickness increases, the maximum critical Rayleigh number decreases. It also suggests that the maximum critical Rayleigh number is bounded for small $d_{l,u}$.

In figure 10, we show a phase diagram for boundary thicknesses $0.1 \leqslant d_{l,u} \leqslant 1.0$ and for $0 \leqslant \gamma \leqslant 50.0$. This figure, for which $\lambda_{l,u} = \eta_{l,u} = 1.0$, shows the boundaries between the three types of bifurcations that can occur in this system. The phase diagrams for different values of conductivity and diffusivity ratio can be quite different. A point worth mentioning is that the critical numbers can be discontinuous across the phase boundaries. For example, the critical wavenumber, a_c, and the critical Hopf frequency, σ_c, are discontinuous across all of the three phase boundaries shown in figure 10.

In the following sections we explore the effect of changing the thermal conductivity ratio, thermal diffusivity ratio and the differential gain on the maximum critical Rayleigh number. To do so, we must choose a reasonable boundary thickness. Given the results of this section, we choose a boundary thickness of $d = 0.25$ unless otherwise noted. This is thin enough that the controller can have a significant influence on the critical state yet thick enough that reliable experimental apparatus may be built.

3.2. *Thermal conductivity ratio*

In this section we fix the boundary thicknesses to $d_{l,u} = 0.25$, hold the thermal diffusivity ratios to $\eta = 1.0$ and change both the proportional gain and the thermal conductivity ratios, λ. It should be stressed that upon changing the ratio of the thermal conductivities, we must make an inverse-proportional change to the heat capacity ratios so that the thermal diffusivity ratio remains constant. We show, in figure 11, a waterfall plot of critical Rayleigh number for proportional gains between

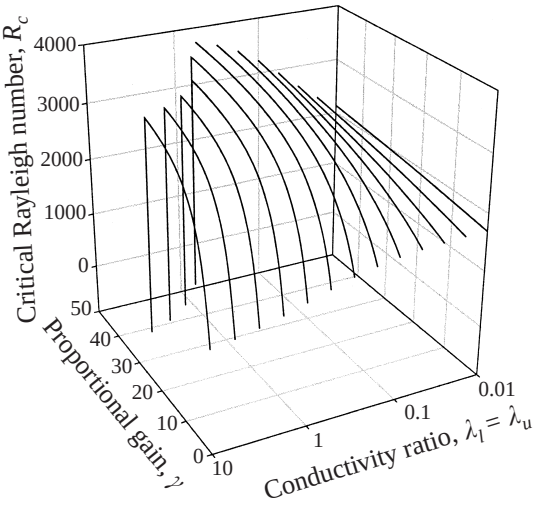

FIGURE 11. Critical Rayleigh number plotted against proportional gain and thermal conductivity ratio, λ. Notice that increasing the thermal conductivity of the boundary material relative to the fluid (small λ) decreases the effectiveness of control through thermal perturbation of the heat flux boundary condition.

0 and 50.0. In the figure, we make twelve uniform steps of $\log(\lambda)$ over three decades. The range of λ is not centred around 1.0. Rather, we choose the values based on common materials used in experiments. With $d_{l,u} = 0.25$ there is no transition $S \rightarrow H_2$ for the range of parameters studied here. Rather, the transition is $S \rightarrow H_i$ with increasing gain.

As was shown by Metcalf & Behringer (1990), the critical Rayleigh number and critical wavenumber for the uncontrolled problem both change when one changes the ratio of thermal conductivities of the boundary material and fluid. For the parameter range considered in figure 11, the effect is small. However, when we add active control through perturbation of the lower boundary heat flux, the effect of conductivity ratio amplifies the change in critical values. Figure 11 shows that reducing the thermal conductivity ratio (decreasing the fluid conductivity or increasing the boundary conductivity) reduces the overall change in the critical Rayleigh number with increased proportional gain. This may be understood if one considers a temperature perturbation of some amplitude made at the lower boundary in a system with small λ. In this case the fluid is insulating and most of the overall temperature drop will occur across the fluid layer rather that across the bounding plates. As a result, the temperature perturbation made on the lower side of the boundary is diminished at the fluid–solid interface. Of course, by decreasing the thickness ratio this problem is assuaged. These results suggest that control experiments should generally have conductivity ratios of order 1.0.

3.3. *Thermal diffusivity ratio*

In this section, we explore the effects of changing the thermal diffusivity ratio $\eta_{l,u}$ with the other parameters held fixed. Before we present critical values, some discussion of the role one might expect the thermal diffusivity ratio to play is needed. By inspecting the linear stability equations, (2.8), the thermal and flow boundary conditions (2.11)–(2.15) and (2.19) and the characteristic values (2.10), one can expect the stationary bifurcation to be unaffected by the thermal diffusivity ratio. In fact, the thermal

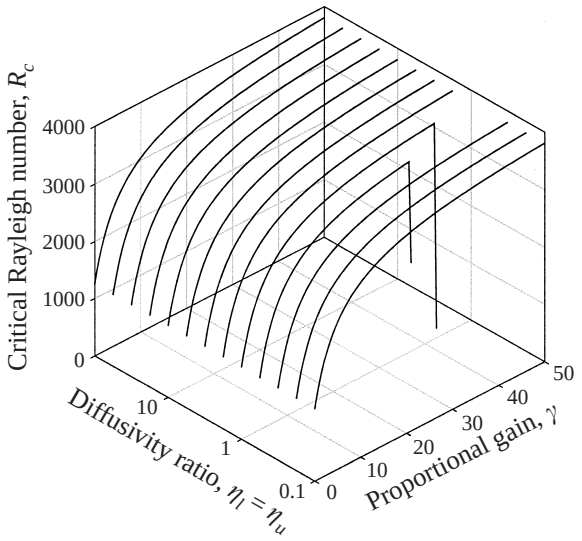

FIGURE 12. Critical Rayleigh number plotted against proportional gain and thermal diffusivity ratio, η. Changing the diffusivity ratio only affects the Hopf bifurcation.

diffusivity ratio only enters the boundary conditions explicitly through the differential gain, (2.21). In this section, though, we will not consider differential gain but prefer to discuss this in § 3.4. The diffusivity ratios enter the solvability condition implicitly through the characteristic values of the solutions to the perturbation equations for the lower x_l and upper x_u boundaries (see (2.10)). Even then, the characteristic values are unaffected if the growth rate is 0. This argument is supported by figure 12 in which we show the critical Rayleigh number as a function of proportional gain and diffusivity ratio. Each of the curves in figure 12 is the same except where the stationary bifurcation gives way to the H_i bifurcation.

Unlike the stationary bifurcation, the location of the Hopf bifurcation is dependent upon the diffusivity ratio. Generally, we find that by increasing the diffusivity ratio, we move the Hopf solution curve to higher Rayleigh number. This can be explained by again considering the thermal diffusion time across the lower boundary. If the boundary thickness is held constant, the diffusion time decreases with increasing diffusivity ratio. This reduces the delay time between measurement and feedback control actuation. By reducing the control actuation delay, we decrease the likelihood of overstable control actuation. An alternative to the system considered here would use an insulating boundary and place the actuators (heaters) at the fluid–solid interface. This should considerably decrease actuation inertia. However, this may not be practical for some experiments or devices.

3.4. *Differential gain*

The final parameter we explore is the differential gain. Since the differential gain only acts on the time-dependent signal from the shadowgraph, this parameter will only affect the H_2 and H_i states and will have no influence on the bifurcation to stationary convection. This may allow the experimentalist to select boundary materials properties based on other design points and delay time-dependent bifurcations via differential gain.

First, we will explore the behaviour of the H_i bifurcation for the case of $d_{l,u} =$

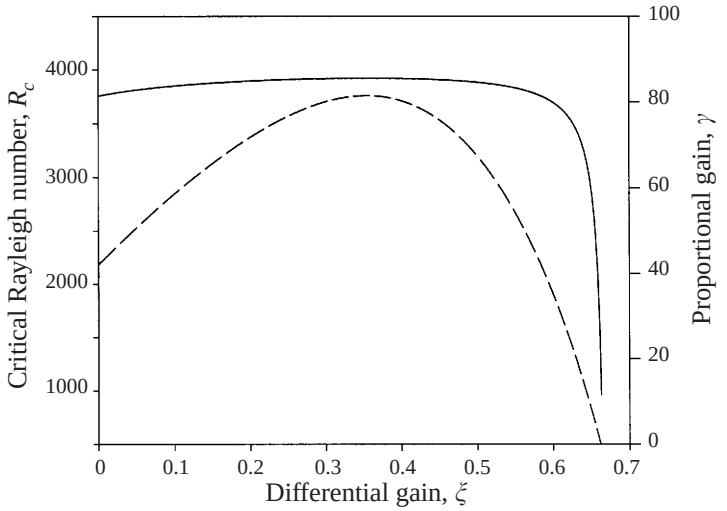

FIGURE 13. Maximum critical Rayleigh (solid line, left axis) and proportional gain (broken line, right axis) plotted against differential gain, ξ, for the transition $S \rightarrow H_i$. The boundary thickness used for these solutions is $d_{l,u} = 0.25$ while the boundary conductivity and diffusivity are equal to the corresponding values of the fluid ($\lambda_{l,u} = \eta_{l,u} = 1.0$).

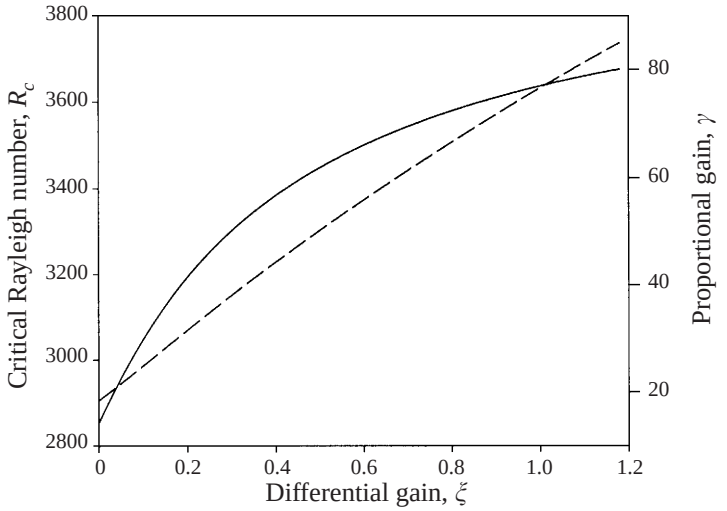

FIGURE 14. Maximum critical Rayleigh (solid line, left axis) and proportional gain (broken line, right axis) plotted against differential gain, ξ, for the transition $S \rightarrow H_2$ (see figure 2). A boundary thickness of $d_{l,u} = 0.5$ is used for these data. The conductivity and diffusivity ratios for these curves are $\lambda_{l,u} = \eta_{l,u} = 1.0$.

0.25. For this and the H_2 problem, the maximum critical Rayleigh number occurs immediately before the transition from S to H bifurcation. If we are able to delay the H states, then the greater proportional gain permitted by some amount of differential gain will allow greater critical Rayleigh numbers in the S state. Figure 13 shows the maximum critical Rayleigh number and the proportional gain at transition from S to H_i bifurcation. One can see from the figure that the differential gain allows some additional amount of proportional gain but only slightly so. Also shown in

the figure is the fact that too great an amount of differential gain will lower the maximum proportional gain and therefore the maximum critical Rayleigh number. This is probably due to the fact that differential gain can amplify noise in the system.

In figure 14, the maximum critical Rayleigh number and proportional gain are plotted against the differential gain. This figure is similar to the previous figure except that the transition explored is $S \rightarrow H_2$. For this calculation, we use a boundary thickness of $d_{l,u} = 0.5$ and conductivity and diffusivity ratios of $\lambda_{l,u} = \eta_{l,u} = 1.0$ This choice of boundary properties removes the isola from the set of possible critical points thus guaranteeing the transition $S \rightarrow H_2$. For each point in figure 14, the stationary and time-dependent minima are balanced. When we increase the differential gain, the time-dependent solution moves toward greater R. We can then increase the proportional gain to balance the minima. The net result (shown in figure 14) is that greater proportional gain is possible and the maximum critical Rayleigh increases.

4. Conclusions

In this paper, we use linear stability analysis to explore the role the horizontal boundary material properties play in selecting the critical state in controlled Rayleigh–Bénard convection in a horizontally infinite domain. The properties we explore are the thickness ratio, the thermal conductivity ratio, and the thermal diffusivity ratio. We only consider the case of symmetric boundary properties. The Prandtl and Biot numbers, although most certainly playing an important role, are held fixed here. A key finding of this work is that the horizontal boundaries introduce a control actuation delay into the dynamics of convection onset. This can give rise to a primary Hopf bifurcation to time-dependent convection. Without consideration of the boundaries, even with the proportional control considered here, only stationary primary bifurcations are found (Howle 1997*c*). The most surprising finding of this study is the appearance of an isola to time-dependent convection at onset for certain parameter ranges.

The thickness of the horizontal bounding plates, when compared to the height of the fluid layer, has considerable influence on both the S and H bifurcations. Generally, we recommend thin boundaries for control experiments. There are, however, two points that argue against the use of thin plates. One point is the need for uniform fluid layer height (flat boundaries). It is difficult to maintain flat boundaries with thin plates, especially with the non-uniform thermal strains created by active control of the heat flux distribution. A second more subtle point involves the critical point through isola formation. We find that at certain boundary thicknesses, the saddle and isola points meet and annihilate one another at a higher-order isola birth point. Increasing the boundary thickness above this value will guarantee that the critical state is either S or H_2 and never H_i. These points not withstanding, as one uses thicker boundaries, the amount by which convection onset is delayed decreases.

We find that the thermal conductivity ratio affects both the S and H critical points. Without control, the conductivity ratio is known to shift the critical Rayleigh number and wavenumbers. In the presence of control, a greater critical Rayleigh number is possible with greater λ (fluid conductivity greater than the boundary conductivity). However, at higher conductivity ratios, an isola to time-dependent convection becomes possible for smaller proportional gains. As the boundary becomes much more conductive, feedback control becomes ineffective. We, therefore, find that a conductivity ratio of $O[1]$ to be a reasonable recommendation.

The thermal diffusivity ratio affects only the time-dependent critical points and not the stationary critical point. In general, the H_2 or H_i critical point shifts to higher critical Rayleigh number as the diffusivity ratio increases. This allows the controller to use greater proportional gain and delay the stationary bifurcation further. These facts point toward higher diffusivity materials for the boundaries of convection control experiments.

The final point studied in this work is the addition of differential gain to the control law. Differential gain only affects the time-dependent critical points. We find that some additional delay of the onset of convection is afforded by using differential gain.

I would like to thank Tesfay Meressi and the reviewers for their constructive comments. Acknowledgment is made to the Donors of The Petroleum Research Fund, administered by the American Chemical Society, for support of this work through grant ACS-PRF# 31645-G9.

REFERENCES

Cerisier, P., Rahal, S., Cordonnier, J. & Lebon, G. 1998 Thermal influence of boundaries on the onset of Rayleigh–Bénard convection. *Intl J. Heat Mass Transfer* **41**, 3309–3320.

Davis, S. H. 1976 The stability of time periodic flows. *Ann. Rev. Fluid Mech.* **8**, 57–74.

Gad-el-Hak, M. 1996 Modern developments in flow control. *Appl. Mech. Rev.* **49**, 365–379.

Gresho, P. M. & Sani, R. L. 1970 The effects of gravity modulation on the stability of a heated fluid layer. *J. Fluid Mech.* **40**, 783–806.

Gustafson, M. R. & Howle, L. E. 1999 Effects of anisotropy and boundary plates on the critical values of a porous medium heated from below. *Intl J. Heat Mass Transfer* **42**, 3419–3430.

Howle. L. E. 1997*a* Control of Rayleigh–Bénard convection in a small aspect ratio container. *Intl J. Heat Mass Transfer* **40**, 817–822.

Howle, L. E. 1997*b* Active control of Rayleigh–Bénard convection. *Phys. Fluids* **9**, 1861–1863.

Howle, L. E. 1997*c* Linear stability analysis of controlled Rayleigh–Bénard convection using shadowgraphic measurement. *Phys. Fluids* **9**, 3111–3113.

Howle, L. E., Behringer, R. P. & Georgiadis, J. G. 1997 Convection and flow in porous media. Part 2. Visualization by shadowgraph. *J. Fluid Mech.* **332**, 247–262.

Kubiček, M. & Marek, M. 1984 *Computational Methods in Bifurcation Theory and Dissipative Structures* (ed. H. Cabannes, M. Holt, H. B. Keller, J. Killeen & S. A. Orszag). Springer.

Metcalf, G. P. & Behringer, R. P. 1990 Critical Rayleigh numbers for cryogenic experiments. *J. Low Temp. Phys.* **78**, 231–246.

Müller, G. 1988 *Crystals: Growth, Properties, and Applications; 12: Convection and Inhomogeneities in Crystal Growth from the Melt* (ed. T. Arizumi, W. Bardsley, H. Bethge *et al.*). Springer.

Rosenblat, S. & Herbert, D. M. 1970 Low-frequency modulation of thermal instability. *J. Fluid Mech.* **43**, 385–398.

Rosenblat, S. & Tanaka, G. A. 1971 Modulation of thermal convection instability. *Phys. Fluids* **14**, 1319–1322.

Tang, J. & Bau, H. H. 1993*a* Stabilization of the no-motion state in Rayleigh–Bénard convection through the use of feedback control. *Phys. Rev. Lett.* **70**, 1795–1798.

Tang, J. & Bau, H. H. 1993*b* Feedback control stabilization of the no-motion state of a fluid confined in a horizontal, porous layer heated from below. *J. Fluid Mech.* **257**, 485–505.

Tang, J. & Bau, H. H. 1994 Stabilization of the no-motion state in the Rayleigh–Bénard problem. *Proc. R. Soc. Lond.* A **447**, 587–607.

Tang, J. & Bau, H. H. 1995 Stabilization of the no-motion state of a horizontal fluid layer heated from below with Joule heating. *Trans. ASME: J. Heat Transfer* **117**, 329–333.

Tang, J. & Bau, H. H. 1998 Experiments on the stabilization of the no-motion state of a fluid layer heated from below and cooled from above. *J. Fluid Mech.* **363**, 153–171.

Thess, A. & Orszag, S. A. 1995 Surface-tension-driven Bénard convection at infinite Prandtl number. *J. Fluid Mech.* **283**, 201–229.

Venezian, G. 1969 Effect of modulation on the onset of thermal convection. *J. Fluid Mech.* **35**, 243–254.

Yih, C.-S. & Li, C.-H. 1972 Instability of unsteady flows or configurations. Part 2. Convective instability. *J. Fluid Mech.* **54**, 143–152.